A cross-layer optimization based integrated routing and grooming algorithm for green multi-granularity transport networks

Xingwei Wang [a,*], Hui Cheng [b], Keqin Li [c], Jie Li [d], Jiajia Sun [a]

[a] College of Information Science and Engineering, Northeastern University, Shenyang 110819, China
[b] Department of Computer Science and Technology, University of Bedfordshire, Luton LU1 3JU, United Kingdom
[c] Department of Computer Science, State University of New York, New Paltz, NY 12561, USA
[d] Department of Computer Science, University of Tsukuba, Tsukuba Science City, Ibaraki 305-8573, Japan

HIGHLIGHTS

- A novel cross-layer optimization model is developed for power-efficient MTN.
- A green integrated routing and grooming algorithm is developed based on BBO.
- Both the power consumption and the multi-user QoS satisfaction degree are optimized.

ARTICLE INFO

ABSTRACT

With the development of IP networks and intelligent optical switch networks, the backbone network tends to be a multi-granularity transport one. In a multi-granularity transport network (MTN), due to the rapid growth of various applications, the scale and complexity of network devices are significantly enhanced. Meanwhile, to deal with bursty IP traffic, the network devices need to provide continuous services along with excessive power consumption. It has attracted wide attention from both academic and industrial communities to build a power-efficient MTN. In this paper, we design an effective node structure for MTN. Considering the power savings on both IP and optical transport layers, we propose a mathematical model to achieve a cross-layer optimization objective for power-efficient MTN. Since this optimization problem is NP-hard (Hasan et al. (2010) [11]) and heuristic or intelligent optimization algorithms have been successfully applied to solve such kinds of problems in many engineering domains (Huang et al. (2011) [13], Li et al. (2011) [17] and Dong et al. (2011) [5]), a Green integrated Routing and Grooming algorithm based on Biogeography-Based Optimization (Simon (2008) [23]) (GRG_BBO) is also presented. The simulation results demonstrate that, compared with the other BBO based and state-of-the-art power saving approaches, GRG_BBO improves the power savings at a rate between 2%–15% whilst the high-level multi-user QoS (Quality of Services) satisfaction degree (MQSD) is guaranteed. GRG_BBO is therefore an effective technique to build a power-efficient MTN.

© 2013 Elsevier Inc. All rights reserved.

1. Introduction

Increasingly mature technologies in IP and intelligent switch optical networks result in a huge amount of switching traffic and wavelengths in fibers. Correspondingly, the optical cross-connect (OXC) has a more complicated structure, and the network stability and reliability becomes rather poor [4]. Furthermore, a traditional OXC only supports the wavelength-level traffic but hinders the coarser granularity (e.g., waveband) transmission. This problem also restrains the processing speed of the network nodes

and becomes the bottleneck in developing a high-speed switching technology. To solve the above problem and to implement a seamless integration of IP and optical transport networks, the multi-granularity switching mechanism is necessary to be introduced to build a multi-granularity transport network (MTN) [4]. MTN is an effective network structure equipped with a simple node structure for reducing the power consumption cost. In MTN, various granularity-levels demand (e.g., IP traffic, wavelength, waveband, and even fiber) transmissions are utilized. Ideally, each intermediate node merely needs one optical switching port to transmit traffic. Therefore, the transmission efficiency and network throughput are improved in the optical transport layer.

The greenhouse effect is aggravated due to increasing power consumption. It is reported that the reduction of 1% power

* Corresponding author.
  E-mail address: wangxw@mail.neu.edu.cn (X. Wang).

consumption saves 5 billion dollars per year [22]. Designing a power-efficient MTN has attracted wide attention from both academic and industrial communities. Overall, there are two factors of excessive power consumption in an MTN. One factor is the expanding network scale and service ranges driven by the rapid growth of various applications. The other factor is that the network devices need to provide continuous services to deal with burst IP traffic and that redundant links and devices are required to guarantee network reliability. However, due to low link or device utilization, a huge amount of power used for network transmission is wasted [32]. In this paper, we study how to improve the power saving for an MTN whilst its advantages are still fully exploited. We have two roadmaps to reduce power consumption, i.e., achieving power saving from the device level and from the system level.

For device-level power saving, a primary strategy is to reduce the power consumption in devices by introducing novel manufacturing technologies or power aware modules. For system-level power saving, the primary strategies are traffic reorganization, power aware routing, and hybrid grooming (e.g., traffic grooming with an optical bypass). In traffic reorganization, an effective approach of traffic migration and rerouting lets more devices in the system turn into the idle state and then fall into sleep mode or even be shut down. Power aware routing aims to select a path along with fewer number of routing hops traversed. Hybrid grooming is able to multiplex several IP-level demands from the IP layer into a high-capacity optical tunnel by traffic grooming. Meanwhile, an optical bypass without optical–electrical–optical (OEO) conversion is implemented on the optical layer. Thereby hybrid grooming reduces the power consumption by IP router ports and OEO conversions.

Note that device-level power savings are constrained by the slow development of manufacturing technologies. As a typical system-level power saving method, the issue of green integrated network routing and grooming has become the research focus on designing future power-efficient MTN. Specially, to achieve the globally optimal network power efficiency, a green integrated routing and grooming algorithm should jointly utilize various power saving strategies such as traffic reorganization, hybrid grooming, waveband switching, and intelligent routing. Furthermore, it also needs to consider the coordination and cooperation between the cross-layer devices and links of the whole network.

To support cross-layer optimization based and power-efficient MTN, we propose a novel green integrated routing and grooming algorithm based on biogeography-based optimization, which we call GRG_BBO. To the best of our knowledge, this paper is the first work addressing cross-layer optimization in green MTN. The major contributions of this paper are listed as follows.

(1) We propose a novel node structure for MTN. At the IP layer, the core router module has the functionalities of power awareness and management. At the optical transport layer, a multi-granularity optical cross-connect (MG-OXC) structure is deployed to support switching the traffic at granularities larger than a single wavelength. The sparse deployment of wavelength converters is cost-efficient and guarantees the wavelength continuity.

(2) We describe a new type of traffic matrix. In such a matrix, an element not only records the traffic between a network node pair, but also considers user diversity, i.e., recording the required QoS (Quality of Services) level mapped into the application type of each user.

(3) We present a new metric, namely, a power consuming coefficient, which is the ratio of the actual power consumption over the maximum power consumption, to evaluate network power efficiency. Furthermore, we introduce a new concept of multi-user QoS satisfaction degree (MQSD) by considering the diversity of different users' QoS satisfaction degrees. A QoS weighting coefficient matrix is constructed to form a mapping between

various application types and various required QoS satisfaction degrees.

(4) We design a layered auxiliary graph (LAG) based on the node structure in MTN to support GRG_BBO. In LAG, the reasonable edge weight is set and multiple candidate paths are calculated on LAG for each demand. Meanwhile, our LAG helps to generate an initial solution for BBO.

(5) GRG_BBO uses the traffic reorganization technique (e.g., load migration and adaptive sleeping) in the core router module. The traffic on the lightly loaded devices is transferred into heavily loaded ones. Thus, more devices in the core router module are turned into the idle state and the corresponding power is saved at the IP layer.

(6) GRG_BBO effectively combines hybrid grooming with waveband switching. Hybrid grooming is used to achieve power efficiency at the IP layer. Waveband switching is used for switching port saving at the optical transport layer.

(7) GRG_BBO can further improve the effectiveness of both hybrid grooming and waveband switching by using intelligent BBO. Finally, global cross-layer optimization of both power consumption and MQSD is achieved.

2. Related work

2.1. Literature review

Although the issue of power saving has attracted a lot of interest, little research has been done on green integrated routing and grooming in MTN. Simulation results given in [2] have predicted the trend of power consumption in the next generation Internet, where the core network consumes most of the power. As one of the primary elements in the core network, cross-layer optimization of a power-efficient design of MTN is emphasized. However, no effective green integrated routing and grooming algorithms are presented in [2].

For device-level power saving, the primary strategies include the manufacturing technologies improvement in the reduction of the device scale and power consumption [8,19], and the adaptive load migration and fast sleeping of the devices [21,7]. However, the slow innovation of manufacturing technologies and the high complexity of introducing relevant function modules hinder the development and production of highly power-efficient devices. For system-level power saving, traffic reorganization schemes [1,25,15,14] have been proposed for the IP layer and the optical transport layer in the MTN. At the IP layer, dynamic rerouting methods are quite popular. The main idea is to transfer the traffic on lightly loaded devices to heavily loaded ones. Idle devices fall into sleep mode or are turned off to save power in the IP network [25]. At the optical transport layer, traffic switching among different lightpaths is proposed in [15,14]. In this method, traffic on one lightpath is tuned to the idle spectrum of another lightpath. This way, the traffic on the previous lightpath was vacated and the associated interfaces are turned off to save power at the optical transport layer. However, traffic reorganization schemes make the network topology dynamically changing, which worsens the delay and error rate.

Most of previous research on power aware routing focused on wireless networks, where the power supplement of each node is constrained. Since MTN is a wired network, the limited supplement of power is not an important issue. Only a few papers [10,29] have proposed adaptive routing algorithms in wired networks to calculate the lower power-consuming paths. However, adopting power saving strategies at the IP layer only is not the final step. This motivates us to transfer more traffic from the IP layer onto the optical transport layer. That is, the cross-layer optimization design

based on green integrated routing and grooming is necessary to be investigated.

With regard to power-efficient grooming, Shen [22] proposed a hybrid grooming based power saving strategy by investigating the unique features of MTN. By using this strategy, multiple IP-level demands are groomed into a high-capacity lightpath bypassing all of the intermediate nodes at the optical transport layer. Thus, both the number of used IP router ports and the number of OEO conversions are reduced to save power. Overall, there are mainly two categories of approaches for implementing power saving based on hybrid grooming. They are (1) maximizing the power saved from hybrid grooming and (2) minimizing the power consumption by establishing lightpaths. In the first category, Shen and Yetginer [22,31] proposed a hybrid grooming strategy with the reduction of power consumption in the electrical interfaces at the IP layer and the OEO conversions. Furthermore, an integer linear programming (ILP) model was used to solve the above problem. Xia [30] proposed an auxiliary graph based hybrid grooming where the edge weight is set by the power usage. Based on this auxiliary graph, optical bypass, traffic grooming, and hybrid grooming were respectively implemented. Simulation results demonstrated that hybrid grooming obtains the best effect of power saving. In the second category, Cao et al. [4] have studied the power aware hybrid grooming problem and proposed auxiliary-graph-based heuristics. By using the current active components in core routers as much as possible, a heuristics proposed in [4] can increase the number of components with idle states, so that the power consumption in establishing the lightpaths decreases. However, these existing approaches are restricted by each other. In particular, the improvement of power saving by using hybrid grooming could increase the power consumed by establishing lightpaths, and vice versa. Thus, it is necessary to introduce more effective sub-strategies and integrate them into hybrid grooming for further improving the network power efficiency.

Waveband switching is an effective way of reducing the power consumed by establishing lightpaths. It can bind multiple lightpaths into a waveband tunnel with more than two physical hops and transmit them as a single unit to reduce the power consumption in the optical switching ports. To support waveband switching in a power-efficient routing, several waveband merging schemes were proposed [16,20,18,9]. Among which, the sub-path scheme [9] has the best effect on port saving. In this scheme, multiple lightpaths which traverse the common links can be grouped. Therefore, a joint utilization of hybrid grooming and waveband switching is promising. In this context, Wang and Hou [27,12,28] proposed a concept of integrated grooming, in which after grooming IP-level demands into the lightpaths, the network lightpaths are selectively merged into the waveband tunnels. However, the current research on integrated grooming aims to reduce the network expenditure and has not addressed the power saving in MTN.

Overall, the aforementioned traffic reorganization, power-efficient routing, and grooming methods are independent of each other. Furthermore, they are only restricted to either the IP layer or optical transport layer and no cross-layer optimization has been studied. A green integrated routing and grooming algorithm for future MTN needs to integrate the traffic reorganization, power-efficient routing, hybrid grooming, and waveband switching during the green transmission of multi-granularity demands. Moreover, a cross-layer optimization oriented green integrated routing and grooming can further improve the network power efficiency with the help of effective intelligent optimization techniques.

2.2. Biogeography-based optimization (BBO)

The reference model of the BBO is orthogonal to an ecological system along with multiple habitats. The habitat suitability index (HSI) measures the suitability of one habitat for the survival of ecological populations. Different habitats have different HSIs. BBO relies on the key operations of population migration between different habitats as well as population mutation to globally optimize the whole ecological system. HSI is an important metric used to decide if population migration and mutation are executed in a habitat. In a habitat with a higher HSI, when the number of its population has arrived at a certain level, some population migrates into a neighboring habitat although its HSI is lower. Thus, the superior features of the accepted population exist both in this neighboring habitat and the original habitat. As such, these superior features are maintained and even further expanded. In addition, when the superior features are introduced into the neighboring habitat, the corresponding HSI is increased. Finally, the whole ecological system is driven to evolve towards the direction of obtaining higher HSI values. If the HSI of one habitat remains low, the population in this habitat generates mutation to enhance the population diversity.

3. Problem description

3.1. Network model

An MTN is represented as a connected graph $G = (V, E)$, where V is a set of nodes and E is a set of links. Fig. 1 shows the node structure consisting of a core router module, optical transceivers, and an MG-OXC. These devices have the power awareness and management functions. The core router module deals with the IP-level demands and includes the line cards and chassis. Each line card owns multiple ports and each chassis has multiple line cards. The core router module implements the traffic aggregation, storage, and forwarding through the master engine, forwarding engine, and switching matrix. Optical transceivers mean a pair of one optical transmitter and one optical receiver. The traffic transferring between the IP layer and the optical transport layer is performed in optical transceivers. The MG-OXC handles the optical demands with different granularities. Correspondingly, the MG-OXC has three granular types of cross-connect matrices, i.e., wavelength cross-connect (WXC), waveband cross-connect (BXC), and fiber cross-connect (FXC).

The MG-OXC also has de/multiplexing devices to implement the separation and grouping of multi-granularity demands. The wavelength converters are sparsely deployed in MG-OXC to save network expenditure and power consumption. In the novel node structure above, the traffic from the lightly loaded chassis, line cards, or ports can be vacated, and then the idle devices are scheduled to sleep. The power saving at the IP layer is thereby achieved. The deployment of MG-OXC implements waveband-level routing and reduces the optical switching ports. The power saving at the optical transport layer is thereby achieved. For any link $e_{i,j}$, optical amplifiers are deployed at its two end nodes to strengthen the transmission power-level and the sensitivity degree of optical signals. In addition, as shown in Fig. 2, at every certain physical distance along a fiber link, both in-line optical amplifiers and optical regenerators are deployed to compensate and rectify power loss and distortion of optical signals during long-distance transmission.

The power consuming and QoS parameters used in this paper are defined in Table 1. These parameters are actually input parameters of our optimization problem. Table 2 uses Boolean variables to mark the status of devices, that is, 0 means idle and 1 means active. These parameters are output parameters of our problem.

3.2. Mathematical models

3.2.1. Traffic characterization

The traffic characterization in MTN describes the user's requirements over the network resources and QoS parameters. Based on the DiffServ model [3] and referring to the ITU-
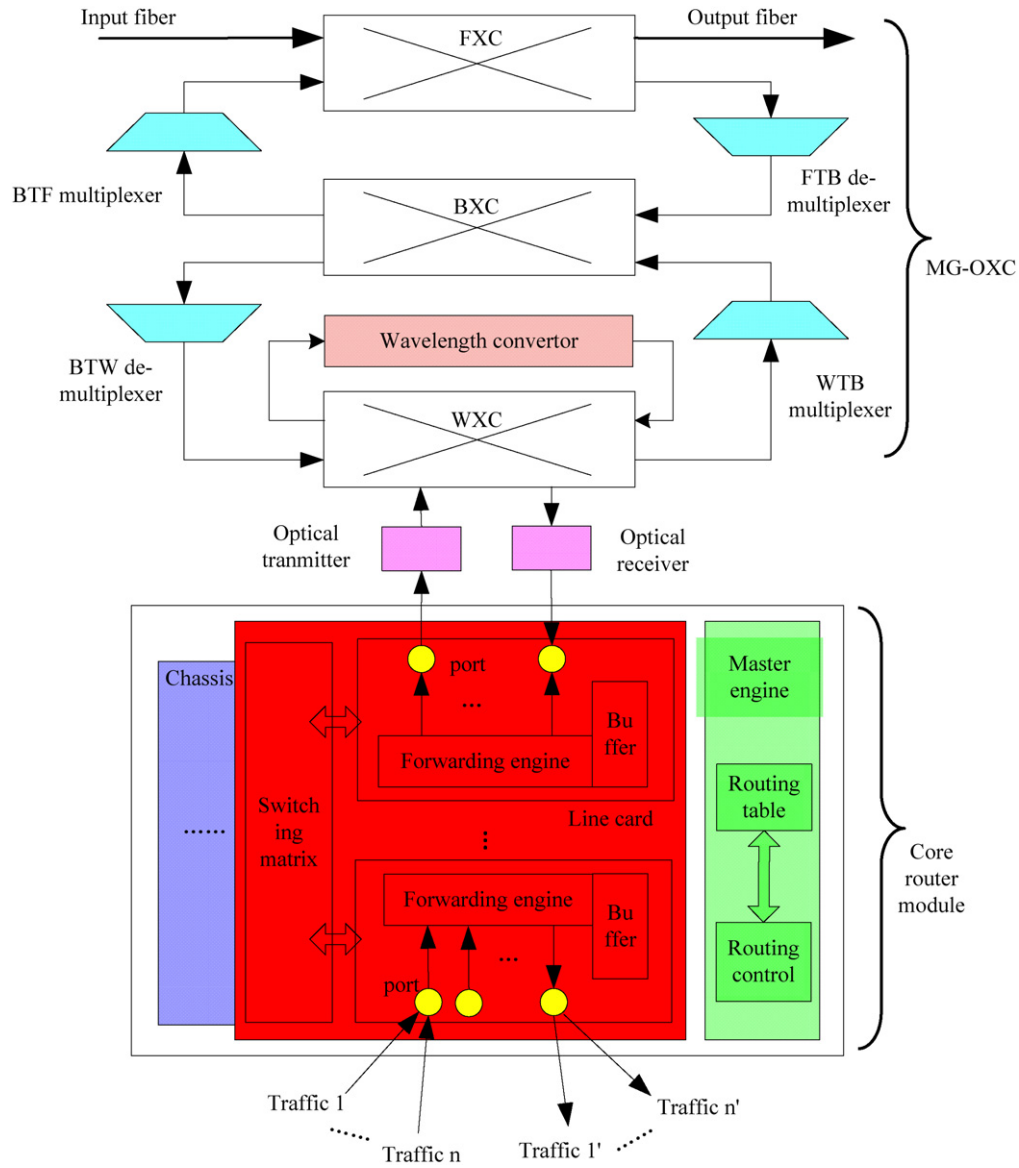
Fig. 1. The node structure in MTN.
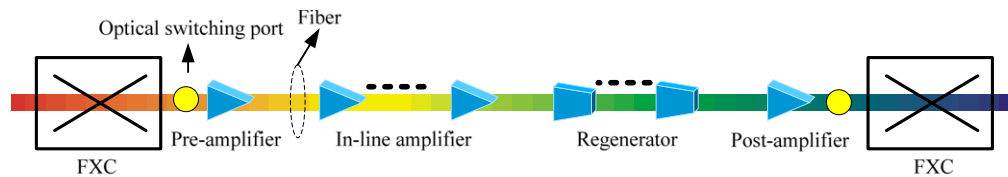
Fig. 2. The link structure in MTN.

TG.1010 document [6], we illustrate 18 different types of available applications in MTN. Each application type t ($t \in [1, 18]$) corresponds to one Q_oS_t, which is a set of different QoS parameter requirements. In this paper, four types of QoS parameters are involved, i.e., bandwidth, delay, delay jitter, and error rate. We have $QoS_t = (\Delta bw_t, \Delta dl_t, \Delta jt_t, \Delta er_t)$. The four elements represent the corresponding QoS parameter requirements of traffic with application type t in terms of bandwidth, delay, delay jitter, and error rate, respectively, where $\Delta bw_t = [bw\_l_t, bw\_h_t]$, $\Delta dl_t = [dl\_l_t, dl\_h_t]$, $\Delta jt_t = [jt\_l_t, jt\_h_t]$, and $\Delta er_t = [er\_l_t, er\_h_t]$. We

define a unicast traffic matrix $R = [r_{sd}]_{|V| \times |V|}$, where $r_{sd} (QoS_t)$ represents the unicast traffic with application type t from the source node v_s to the destination node v_d.

Given the traffic matrix R, we calculate multiple sets of candidate paths used to transmit various types of traffic in R. The optimal set of candidate paths is the optimal solution for R. There are two steps to evaluate a candidate path set. First, we evaluate its power efficiency. We introduce an important metric, power consuming coefficient, to quantify the network power efficiency. It is the ratio of the actual power consumption to the maximum

Table 1
Input parameters of our problem.

Name	Description	Name	Description
P_{ctr}^{cr}	Power consumption of a master engine in the core router module	Dl_{rg}	Delay of regenerating an optical signal
P_{chas}^{cr}	Power consumption of a chassis in the core router module	Dl_t	Transmission delay
P_{lc}^{cr}	Power consumption of a line card in the core router module	$Jt(e_{ij})$	Delay jitter on e_{ij}
P_{port}^{cr}	Power consumption of a port in the core router module	$Er(v_i)$	Error rate of v_i
$P_{b\_port}^{cr}$	Power consumption of a unit bandwidth for a core router port	$N_{chas}^{v_i}$	Number of chassis at v_i
$P_{b\_port}^{wxc}$	Power consumption of a unit bandwidth for a wavelength switching port	$N_{lc}^{v_i,j}$	Number of line cards on the jth chassis at v_i
$P_{b\_port}^{bxc}$	Power consumption of a unit bandwidth for a waveband switching port	$N_{port}^{v_i,j,k}$	Number of ports on the kth line card of the jth chassis at v_i
$P_{b\_port}^{fxc}$	Power consumption of a unit bandwidth for a fiber switching port	$N_t^{v_i}$	Number of optical transmitters at v_i
P_t	Power consumption per optical transmitter	$N_r^{v_i}$	Number of optical receivers at v_i
P_r	Power consumption per optical receiver	$N_{wtb}^{v_i}$	Number of Wavelength To waveBand (WTB) multiplexers at v_i
P_{mux}	Power consumption per multiplexer	$N_{btf}^{v_i}$	Number of waveBand To Fiber (BTF) multiplexers at v_i
P_{demux}	Power consumption per de-multiplexer	$N_{ftb}^{v_i}$	Number of Fiber to waveBand (FTB) de-multiplexers at v_i
P_{port}^{wxc}	Power consumption per wavelength switching port	$N_{btw}^{v_i}$	Number of waveBand to Wavelength (BTW) de-multiplexers at v_i
P_{port}^{bxc}	Power consumption per waveband switching port	$N_{port}^{v_i,wxc}$	Number of wavelength switching ports at v_i
P_{port}^{fxc}	Power consumption per fiber switching port	$N_{port}^{v_i,bxc}$	Number of waveband switching ports at v_i
P_{wc}	Power consumption per wavelength converter	$N_{port}^{v_i,fxc}$	Number of fiber switching ports at v_i
P_{pre}	Power consumption per pre-amplifier	$N_{relay}^{e_{ij}}$	Number of in-line amplifiers on link e_{ij}
P_{relay}	Power consumption per in-line amplifier	$N_{rg}^{e_{ij}}$	Number of regenerators on link e_{ij}
P_{post}	Power consumption per post-amplifier	W	Number of available wavelengths on each fiber
P_{rg}	Power consumption per optical regenerator	B	Number of available wavebands on each fiber
$Dl_{lc}^{v_i}$	Buffer delay inside the line card at v_i	F	Number of available fibers on each link
$Dl_{r/t}^{v_i}$	Transmitting and reception delay at v_i	WB	Wavelength capacity
$Dl_{mg}^{v_i}$	Multi-granularity grooming delay at v_i	B_{port}^{cr}	Available bandwidth per core router port
$Dl_{wc}^{v_i}$	Wavelength conversion delay at v_i	B_{port}^{wxc}	Available bandwidth per wavelength switching port
Dl_{pre}	Pre-amplification delay	B_{port}^{bxc}	Available bandwidth per waveband switching port
Dl_{relay}	In-line amplification delay	B_{port}^{fxc}	Available bandwidth per fiber switching port
Dl_{post}	Post-amplification delay		

Table 2
Variables (output parameters of our problem).

Name	Description	Name	Description
S^{v_i}	Status of v_i	$S_{b\_wxc\_port}^{v_i,w,\alpha}$	Status of the αth bandwidth unit of the wth wavelength switch port at v_i
$S_{chas}^{v_i,j}$	Status of the jth chassis at v_i	$S_{bxc\_port}^{v_i,b}$	Status of the bth waveband switching port at v_i
$S_{lc}^{v_i,j,k}$	Status of the kth line card of the jth chassis at v_i	$S_{b\_bxc\_port}^{v_i,b,\beta}$	Status of the βth bandwidth unit of the bth waveband switching port at v_i
$S_{port}^{v_i,j,k,p}$	Status of the pth port of the kth line card of the jth chassis at v_i	$S_{fxc\_port}^{v_i,f}$	Status of the fth fiber switching port at v_i
$S_{b\_port}^{v_i,j,k,p,\theta}$	Status of the θth bandwidth unit of the pth port of the kth line card of the jth chassis at v_i	$S_{wc}^{v_i}$	Status of the wavelength converter at v_i
$S_t^{v_i}$	Status of the tth optical transmitter at v_i	$S^{e_{ij}}$	Status of link e_{ij}
$S_r^{v_i}$	Status of the rth optical receiver at v_i	$S_a^{e_{ij}}$	Status of the amplifier a on link e_{ij}
$S_{mux}^{v_i,m}$	Status of the mth multiplexer at v_i	$S_r^{e_{ij}}$	Status of regenerator r on link e_{ij}
$S_{demux}^{v_i,d}$	Status of the dth de-multiplexer at v_i	$S_{b\_fxc\_port}^{v_i,f,\gamma}$	Status of the γth bandwidth unit of the fth fiber switching port at v_i
$S_{wxc\_port}^{v_i,w}$	Status of the wth wavelength switching port at v_i		

power consumption of all the devices in the network. Second, we evaluate the multi-user QoS satisfaction degree (MQSD) of this candidate path set. In the real world, the traffic with different application types has different satisfaction degrees of the QoS parameter requirement. In other words, we need to consider the diversity of the user's satisfaction degrees. Therefore, we introduce a new concept of MQSD. The candidate path set with the highest MQSD and the lowest power consuming coefficient is the optimal solution for R.

3.2.2. Quantitative model of power consuming coefficient

The calculation of the power consuming coefficient mainly depends on how to quantify the actual power consumption in the network. As shown in Fig. 1, when the traffic arrives at the IP layer in MTN, the chassis, line cards, and electrical ports of the core router module are activated sequentially, and then the traffic is aggregated and processed by the master engine. Through the E/O conversion at the optical transmitter, the wavelength-level optical signal is generated and then transmitted into the MG-OXC. Then, this optical signal goes through WXC (wavelength

conversion if necessary), WTB multiplexer, BXC, BTF multiplexer, and finally arrives at FXC. For the IP-level traffic leaving the MTN, a reverse procedure is applied. Therefore, given a traffic matrix R, the node-level power consumption in processing traffic, denoted as $P_p(R)$, includes the power consumption of the core router module $P_{cr}(R)$, the power consumption of the optical transceivers $P_{r/t}(R)$, the power consumption of MG-OXC $P_{mg\_oxc}(R)$, and the power consumption of wavelength converters $P_{wc}(R)$. They are formulated in Eqs. (1)–(5) below:

$$P_p(R) = P_{cr}(R) + P_{r/t}(R) + P_{mg\_oxc}(R) + P_{wc}(R) \tag{1}$$

See Box I.

$$P_{r/t}(R) = \sum_{i=0}^{|V|-1} \sum_{t=1}^{N_t^{v_i}} S_t^{v_i} \times P_t + \sum_{i=0}^{|V|-1} \sum_{r=1}^{N_r^{v_i}} S_r^{v_i} \times P_r \tag{3}$$

See Box II.

$$P_{wc}(R) = \sum_{i=0}^{|V|-1} P_{wc} \times S_{wc}^{v_i}. \tag{5}$$

$$P_{cr}(R) = \sum_{i=0}^{|V|-1} \left(P_{ctr}^{cr} + \sum_{j=1}^{N_{chas}^{v_i}} \left(\begin{array}{l} P_{chas}^{cr} \times S_{chas}^{v_i,j} + \\ \sum_{k=1}^{N_{lc}^{v_i,j}} \left(P_{lc}^{cr} \times S_{lc}^{v_i,j,k} + \sum_{p=1}^{N_{port}^{v_i,j,k}} \left(P_{port}^{cr} + \sum_{\theta=1}^{B_{port}^{cr}} P_{b\_port}^{cr} \cdot S_{b\_port}^{v_i,j,k,p,\theta} \right) \times S_{port}^{v_i,j,k,p} \right) \end{array} \right) \right) \tag{2}$$

Box I.

$$P_{mg\_oxc}(R) = \sum_{i=0}^{|V|-1} \left(\begin{array}{l} \sum_{w=1}^{N_{port}^{v_i,wxc}} \left(P_{port}^{wxc} + \sum_{\alpha=1}^{B_{port}^{wxc}} P_{b\_port}^{wxc} \times S_{b\_wxc\_port}^{v_i,w,\alpha} \right) \times S_{wxc\_port}^{v_i,w} \\ + \sum_{m=1}^{N_{wtb}^{v_i}+N_{btf}^{v_i}} P_{mux} \times S_{mux}^{v_i,m} + \sum_{b=1}^{N_{port}^{v_i,bxc}} \left(P_{port}^{bxc} + \sum_{\beta=1}^{B_{port}^{bxc}} P_{b\_port}^{bxc} \times S_{b\_bxc\_port}^{v_i,b,\beta} \right) \times S_{bxc\_port}^{v_i,b} \\ + \sum_{d=1}^{N_{ftb}^{v_i}+N_{btw}^{v_i}} P_{demux} \times S_{demux}^{v_i,d} + \sum_{f=1}^{N_{port}^{v_i,fxc}} \left(P_{port}^{fxc} + \sum_{\gamma=1}^{B_{port}^{fxc}} P_{b\_port}^{fxc} \times S_{b\_fxc\_port}^{v_i,f,\gamma} \right) \times S_{fxc\_port}^{v_i,f} \end{array} \right) \tag{4}$$

Box II.

The power consumption of link transmission is the sum of the optical amplifier's power consumption and the optical regenerator's power consumption. It is formulated as follows:

$$P_t(R) = \sum_{i=0}^{|V|-1} \sum_{j=0}^{|V|-1} \left(P_{pre} + \sum_{a=1}^{N_{relay}^{e_{ij}}} P_{relay} \times S_a^{e_{ij}} + P_{post} + \sum_{r=1}^{N_{rg}^{e_{ij}}} P_{rg} \times S_r^{e_{ij}} \right). \tag{6}$$

Therefore, we calculate the power consuming coefficient $C_p(R)$, which is the ratio of the actual power consumption $P(R)$ to the maximum power consumption P_{max} (i.e., the total power consumption when all the devices are active) in the network. We have

$$C_p(R) = P(R)/P_{max} \tag{7}$$

$$P(R) = P_p(R) + P_t(R). \tag{8}$$

Obviously, the power consuming coefficient characterizes the network power efficiency. Smaller values of $C_p(R)$ mean higher power efficiency.

3.2.3. Quantitative model of MQSD

The MQSD comes from the combination of various single-user QoS satisfaction degrees for various traffic requests r_{sd} in R. Therefore, we need to calculate the single-user QoS satisfaction degree for each traffic request. The following calculation method is used. In the candidate path set of a given traffic request $r_{sd} \in R$, we collect the actual QoS parameter values on each candidate path and then evaluate these parameter values to construct a single-user QoS satisfaction degree matrix (SQSDM). Then, we randomly select one column from the SQSDM and put them together to generate a multi-user QoS satisfaction degree matrix (MQSDM) for R. Based on this MQSDM, we calculate the MQSD values for various candidate path sets for R.

Given the traffic request $r_{sd} \in R$, the acquisition of actual QoS parameter values on the candidate paths depends on the quantitative method of QoS parameters. The bandwidth of the nth candidate path selected by r_{sd}, denoted as $Bw^n(r_{sd})$, includes the actual bandwidth occupied at the IP layer, $Bw_E^n(r_{sd})$, and the actual bandwidth occupied at the optical transport layer, $Bw_O^n(r_{sd})$. That is

$$Bw^n(r_{sd}) = \sum_{j=1}^{N_{chas}^{v_s}} \sum_{k=1}^{N_{lc}^{v_s,j}} \sum_{p=1}^{N_{port}^{v_s,j,k}} \sum_{\theta=1}^{B_{port}^{cr}} S_{b\_port}^{v_s,j,k,p,\theta}$$

$$+ \sum_{j=1}^{N_{chas}^{v_d}} \sum_{k=1}^{N_{lc}^{v_d,j}} \sum_{p=1}^{N_{port}^{v_d,j,k}} \sum_{\theta=1}^{B_{port}^{cr}} S_{b\_port}^{v_d,j,k,p,\theta} + \sum_{w=1}^{N_{port}^{v_s,wxc}} \sum_{\alpha=1}^{B_{port}^{wxc}} S_{b\_wxc\_port}^{v_s,w,\alpha}$$

$$+ \sum_{w=1}^{N_{port}^{v_d,wxc}} \sum_{\alpha=1}^{B_{port}^{wxc}} S_{b\_wxc\_port}^{v_d,w,\alpha} + \sum_{b=1}^{N_{port}^{v_s,bxc}} \sum_{\beta=1}^{B_{port}^{bxc}} S_{b\_bxc\_port}^{v_s,b,\beta}$$

$$+ \sum_{b=1}^{N_{port}^{v_d,bxc}} \sum_{\beta=1}^{B_{port}^{bxc}} S_{b\_bxc\_port}^{v_d,b,\beta} + \sum_{f=1}^{N_{port}^{v_s,fxc}} \sum_{\gamma=1}^{B_{port}^{fxc}} S_{b\_fxc\_port}^{v_s,f,\gamma}$$

$$+ \sum_{f=1}^{N_{port}^{v_d,fxc}} \sum_{\gamma=1}^{B_{port}^{fxc}} S_{b\_fxc\_port}^{v_d,f,\gamma}. \tag{9}$$

The delay of the nth candidate path selected by r_{sd}, denoted as $Dl^n(r_{sd})$, includes the node processing delay $Dl_p^n(r_{sd})$, and the link transmission delay $Dl_t^n(r_{sd})$. That is

$$Dl^n(r_{sd}) = Dl_p^n(r_{sd}) + Dl_t^n(r_{sd}) \tag{10}$$

$$Dl_p^n(r_{sd}) = Dl_{lc}^{v_s} + Dl_{lc}^{v_d} + Dl_{r/t}^{v_s} + Dl_{r/t}^{v_d} + Dl_{mg}^{v_s}$$

$$+ Dl_{mg}^{v_d} + \sum_{i=0}^{|V|-1} Dl_{wc}^{v_i} \times S_{wc}^{v_i} \tag{11}$$

$$Dl_t^n(r_{sd}) = \sum_{i=0}^{|V|-1} \sum_{j=0}^{|V|-1} \left(\left(Dl_{pre} + \sum_{a=1}^{N_{relay}^{e_{ij}}} Dl_{relay} \times S_a^{e_{ij}} \right. \right.$$

$$\left. \left. + \sum_{r=1}^{N_{rg}^{e_{ij}}} Dl_{rg} \times S_r^{e_{ij}} + Dl_{post} + Dl_t \right) \times S^{e_{ij}} \right). \tag{12}$$

From Eq. (11), we can see that only at the two end nodes of a candidate path will the traffic add/drop processing happen; however, at the intermediate nodes, only the necessary wavelength conversion is performed. The processing delay of other devices does not need to be considered.

The link delay jitter is a kind of additive QoS parameter. Therefore, the delay jitter of the nth candidate path selected by r_{sd}, denoted as $Jt^n(r_{sd})$, is the sum of the delay jitters on all the

occupied links. That is,

$$Jt^n(r_{sd}) = \sum_{i=0}^{|V|-1} \sum_{j=0}^{|V|-1} \left(Jt\left(e_{ij}\right) \times S^{e_{ij}} \right). \tag{13}$$

The error rate is a kind of multiplicative QoS parameter. Therefore, the error rate of the nth candidate path selected by r_{sd}, denoted as $Er^n(r_{sd})$, is calculated as follows:

$$Er^n(r_{sd}) = 1 - \prod_{i=0}^{|V|-1} \left(1 - Er\left(v_i\right)\right) \times S^{v_i}. \tag{14}$$

We first evaluate the obtained QoS parameter information above. Given a traffic request $r_{sd} \in R$ of application type t, for the corresponding QoS parameter $\theta^n(r_{sd})$ on the nth candidate path, the evaluation function $\alpha_{\theta}^{n,t}(r_{sd})$ is defined in Box III where h is a pure positive decimal and θ represents any type of QoS parameter. For example, when θ takes the bandwidth parameter Bw, we have $\alpha_{\theta}^{n,t}(r_{sd}) = \alpha_{Bw}^{n,t}(r_{sd})$, $\theta_{\max}^t = bw\_h_t$, $\theta_{\min}^t = bw\_l_t$, $\theta^n(r_{sd}) = Bw^n(r_{sd})$.

In this paper, the diversity of the users' QoS satisfaction degrees is considered, that is, the traffic of different application types has different requirements over various QoS parameters. For application type t, its QoS weight coefficient matrix is $\left[w_t^{Bw}, w_t^{Dl}, w_t^{Jt}, w_t^{Er}\right]$, where $w_t^{Bw} + w_t^{Dl} + w_t^{Jt} + w_t^{Er} = 1$ and $w_t^{Bw}, w_t^{Dl}, w_t^{Jt}, w_t^{Er} > 0$ should be satisfied. When we calculate N candidate paths for the traffic request r_{sd} of application type t, we can construct the SQSDM for r_{sd} as below:

$$S_{QoS}^t(r_{sd}) = \begin{bmatrix} \dfrac{\alpha_{Bw}^{1,t}(r_{sd})}{BW^t}, & \dfrac{\alpha_{Bw}^{2,t}(r_{sd})}{BW^t}, & \cdots & \dfrac{\alpha_{Bw}^{N,t}(r_{sd})}{BW^t} \\[2mm] \dfrac{\alpha_{Dl}^{1,t}(r_{sd})}{DL^t}, & \dfrac{\alpha_{Dl}^{2,t}(r_{sd})}{DL^t}, & \cdots & \dfrac{\alpha_{Dl}^{N,t}(r_{sd})}{DL^t} \\[2mm] \dfrac{\alpha_{Jt}^{1,t}(r_{sd})}{JT^t}, & \dfrac{\alpha_{Jt}^{2,t}(r_{sd})}{JT^t}, & \cdots & \dfrac{\alpha_{Jt}^{N,t}(r_{sd})}{JT^t} \\[2mm] \dfrac{\alpha_{Er}^{1,t}(r_{sd})}{ER^t}, & \dfrac{\alpha_{Er}^{2,t}(r_{sd})}{ER^t}, & \cdots & \dfrac{\alpha_{Er}^{N,t}(r_{sd})}{ER^t} \end{bmatrix}$$

$$\times \left[w_t^{Bw}, w_t^{Dl}, w_t^{Jt}, w_t^{Er}\right]. \tag{16}$$

Here, $BW^t = \sum_{n=1}^{N} \alpha_{Bw}^{n,t}(r_{sd})$, $DL^t = \sum_{n=1}^{N} \alpha_{Dl}^{n,t}(r_{sd})$, $JT^t = \sum_{n=1}^{N} \alpha_{Jt}^{n,t}(r_{sd})$, and $ER^t = \sum_{n=1}^{N} \alpha_{Er}^{n,t}(r_{sd})$.

We randomly select one column from each SQSDM and put them together to form the MQSDM, denoted as $S_{QoS}(R)$. Therefore, for the traffic matrix R, each candidate path set corresponds to each $S_{QoS}(R)$. The MQSD value $Q(R)$ is used to evaluate the candidate path set. However, it is not enough to describe $Q(R)$ by the average value $E\left[S_{QoS}(R)\right]$ of all the elements in $S_{QoS}(R)$. Meanwhile, we need to consider the variance of MQSD, denoted as $D\left[S_{QoS}(R)\right]$, to guarantee the global optimum of $Q(R)$. Intuitively, both a greater average value and a lower variance value mean a higher MQSD in the whole network. Therefore, $Q(R)$ is calculated as below:

$$Q(R) = E\left[S_{QoS}(R)\right]^{D\left[S_{QoS}(R)\right]}. \tag{17}$$

3.2.4. Optimization objectives

The optimization objectives of this paper are to minimize the power consuming coefficient and to maximize the multi-user QoS satisfaction degree, i.e.,

$$Minimize\ [C_p(R)/Q(R)] \tag{18}$$

under the following constraints:

$$S_{chas}^{v_i,j} \leq \sum_{k=1}^{N_{lc}^{v_i,j}} S_{lc}^{v_i,j,k} \quad \forall i,j \tag{19}$$

$$S_{chas}^{v_i,j} \geq S_{lc}^{v_i,j,k} \quad \forall i,j,k \tag{20}$$

$$S_{lc}^{v_i,j,k} \leq \sum_{p=1}^{N_{port}^{v_i,j,k}} S_{port}^{v_i,j,k,p} \quad \forall i,j,k \tag{21}$$

$$S_{lc}^{v_i,j,k} \geq S_{port}^{v_i,j,k,p} \quad \forall i,j,k,p \tag{22}$$

$$\sum_{w \in b} BW^w \leq C_{e_{ij}}^{f,b}, \quad \forall e_{ij}, \forall b \in f \tag{23}$$

$$\sum_{b \in f} BW^b \leq C_{e_{ij}}^f, \quad \forall e_{ij}, \forall f \in e_{ij} \tag{24}$$

$$\sum_{f \in e_{ij}} BW^f \leq C_{e_{ij}}, \quad \forall e_{ij} \tag{25}$$

$$Bw^n(r_{sd}) \leq bw\_h_t \tag{26}$$

$$Dl^n(r_{sd}) \leq dl\_h_t \tag{27}$$

$$Jt^n(r_{sd}) \leq jt\_h_t \tag{28}$$

$$Er^n(r_{sd}) \leq er\_h_t. \tag{29}$$

Constraints (19) and (21) guarantee that if there is no port/line card in the working status on a line card/chassis, this line card/chassis must be turned into the idle state. Constraints (20) and (22) guarantee that if a port/line card is in the active status, the related line card/chassis must be in the working status. Constraints (23) and (24), and (25) show that the total bandwidth occupied on a wavelength, waveband, and fiber should not exceed the capacity of the waveband, the capacity of the fiber, and the link capacity, respectively. Constraints (26)–(29) guarantee that the total bandwidth, delay, delay jitter, and error rate of a path selected by the traffic request r_{sd} should not exceed their upper bounds of various QoS requirements of r_{sd}. This optimization problem is proved to be NP-hard [11] and the intelligent optimization techniques or heuristic methods can be used to find sub-optimal or fast optimal solutions.

4. A green integrated routing and grooming algorithm based on biogeography-based optimization

In this paper, we propose GRG_BBO, which jointly utilizes traffic reorganization, hybrid grooming, waveband switching, and intelligent BBO. The BBO plays the key role in GRG_BBO. It further improves the power efficiency of the other three strategies, accelerates the global optimization of the network power efficiency and the multi-user satisfaction degree, and facilitates the cross-layer optimization of the power savings. In GRG_BBO, the ecological system represents the solution, i.e., a set of paths, which satisfies all the traffic requests in the traffic matrix R. The solution is initialized through GREEDY path search [26] on our constructed auxiliary graph. A habitat in the ecological system represents a path searched by GRG_BBO for a traffic request $r_{sd} \in R$ on the auxiliary graph. The populations in a habitat represent the links of the path. The habitat suitability index reflects the comprehensive evaluation on the power consuming coefficient and the single-user QoS satisfaction degree (SQSD) of the selected path of r_{sd}. The global HSI of the ecological system reflects the comprehensive evaluation on the power consuming coefficient of the whole network and the MQSD. The prominent advantage of GRG_BBO is to exploit the common links as the superior feature,

$$\alpha_\theta^{n,t}(r_{sd}) = \begin{cases} 1 & \theta^n(r_{sd}) \le \theta_{min}^t \\ \dfrac{\theta_{max}^t - h \times \theta_{min}^t - (1-h) \times \theta^n(r_{sd})}{\theta_{max}^t - \theta_{min}^t} & \theta_{min}^t < \theta^n(r_{sd}) < \theta_{max}^t \\ h & \theta^n(r_{sd}) = \theta_{max}^t \\ 0 & \theta^n(r_{sd}) > \theta_{max}^t \end{cases}$$

(15)

Box III.

and to perform the migration of links (i.e., populations) between the different paths (i.e., habitats). As such, the power efficiency of hybrid grooming and waveband switching is further improved. The mutation operation of links is utilized to enrich the link diversity and to provide more optional paths for GRG_BBO. The superior feature in BBO is maintained and even expanded, thereby the global optimization of the network performance is finally achieved.

4.1. Construction of layered auxiliary graph

We have designed a novel layered auxiliary graph (LAG) which is orthogonal to the layered graph with the functionalities of power awareness and modularized management in [4]. The difference is that the waveband and fiber layers are added into our LAG to support multi-granularity routing. Correspondingly, we transform the green unicast routing issue into the problem of LAG construction. In LAG, the edge weight is set as (Ca, Pc, Dl, Jt, Er), where Ca, Pc, Dl, Jt and Er separately represent the capacity, power consumption, delay, delay jitter, and error rate of the corresponding link. Based on the LAG, we calculate one or multiple candidate paths, each of which satisfies its QoS requirements, for the given traffic request. We illustrate the LAG construction and the candidate path computation on LAG constructed from a simple three-node network topology. As shown in Fig. 3, the detailed method of LAG construction is described as follows.

Step 1: Generate the nodes in LAG according to $v_i \in V$ (the node degree is d_i) in $G(V, E)$. From the bottom access layer to the top fiber layer, the total number of nodes is $2 \times \left(2 + N_{chas}^{v_i} + N_{lc}^{v_i,j} + N_{port}^{v_i,j,k} + F \times d_i + B \times d_i + W \times d_i\right)$.

Step 2: Generate the edges in LAG according to $v_i \in V$ by the following procedure.

Step 2.1: At the access layer, add a grooming edge from the adding node to the dropping node and the edge weight is $(\infty, 0, 0, 0, 0)$. Add an access edge between the access layer node and the chassis layer node and the edge weight is $(\infty, 0, 0, 0, 0)$. Add a chassis edge between the chassis layer node and the line card layer node and the edge weight is $\left(\infty, P_{ctr}^{cr} + P_{chas}^{cr}, 0, 0, 0\right)$. Add a line card edge between the line card layer node and the port layer node and the edge weight is $\left(\infty, P_{lc}^{cr}, Dl_{lc}^{v_i}, 0, 0\right)$. Add a port edge between the port layer node and the transceiver layer node and the edge weight is $\left(\infty, P_{port}^{cr}, 0, 0, 0\right)$.

Step 2.2: Add a transmitting edge and a receiving edge between the transceiver layer node and the wavelength layer node and the edge weights are $\left(WB, P_t + P_{port}^{wxc}, Dl_{r/t}^{v_i}, 0, 0\right)$ and $\left(WB, P_r + P_{port}^{wxc}, Dl_{r/t}^{v_i}, 0, 0\right)$, respectively. Add a multiplexing edge and a de-multiplexing edge between the wavelength layer node and the waveband layer node and the edge weights are $\left(W \cdot WB/B, P_{port}^{wxc} + P_{mux} + P_{port}^{bxc}, 0, 0, 0\right)$ and $\left(W \cdot WB/B, P_{port}^{wxc} + P_{demux} + P_{port}^{bxc}, 0, 0, 0\right)$, respectively. Add a multiplexing edge

and a de-multiplexing edge between the waveband layer node and the fiber layer node and the edge weights are $\left(W \cdot WB, P_{port}^{bxc} + P_{mux} + P_{port}^{fxc}, 0, 0, 0\right)$ and $\left(W \cdot WB, P_{port}^{bxc} + P_{demux} + P_{port}^{fxc}, 0, 0, 0\right)$, respectively.

Step 2.3: At the wavelength layer, waveband layer, and fiber layer, separately add the wavelength bypass edge, waveband bypass edge, and fiber bypass edge from the dropping node to all the adding nodes. The weight of each edge is $(\infty, 0, 0, 0, 0)$. If node v_i has the wavelength conversion function, add a wavelength conversion edge and the edge weight is $\left(\infty, 2 \times P_{port}^{wxc} + P_{wc}, Dl_{wc}^{v_i}, 0, 0\right)$.

Step 3: Generate the links in LAG according to $e_{ij} \in E$ in $G(V, E)$. If link e_{ij} connects v_i and v_j, add a wavelength-link and the link weight is $\left(WB, \ P_{pre} + \sum_{a=1}^{N_{relay}^{e_{ij}}} P_{relay} \times S_a^{e_{ij}} + \sum_{r=1}^{N_{rg}^{e_{ij}}} P_{rg} \times S_r^{e_{ij}} + P_{post}, Dl_{pre} + \sum_{a=1}^{N_{relay}^{e_{ij}}} Dl_{relay} \times S_a^{e_{ij}} + \sum_{r=1}^{N_{rg}^{e_{ij}}} Dl_{rg} \times S_r^{e_{ij}} + Dl_{post} + Dl_t, \ Jt\left(e_{ij}\right), Er\left(v_i\right)\right)$.

Step 4: The construction of LAG is completed.

In the simple three-node topology shown in Fig. 3(a), we make the following assumptions. Each network node is equipped with one chassis. Each chassis has one line card. Each line card has two ports. Only node 3 has the wavelength conversion capability. Each link has two wavelengths, one waveband, and one fiber. The corresponding LAG is constructed by the aforementioned method and it is shown in Fig. 3(b). When we calculate a candidate path for the traffic request r_{13}, the direction mapping of this candidate path on LAG is denoted by the green line in Fig. 3(b). If this candidate path satisfies the waveband merging condition, its following direction mapping is shown by the blue line in Fig. 3(b). We can see that the LAG not only implements the integration of the IP core router devices and the optical OXC devices, but also well supports the joint routing at both the IP layer and optical transport layer.

4.2. Solution representation and initialization

The ecological system $ES_{|V| \times |V|}$ represents the solution matrix. A solution is a path set, which satisfies all the traffic requests in the traffic matrix R. The element in $ES_{|V| \times |V|}$ is denoted as $ES_{ij}\left(HSI_{ij}, N_{ij}\right)$ and represents a path (habitat) from node v_i to node v_j. HSI_{ij} is the habitat suitability index value of ES_{ij} and its computation method is shown in Eq. (30). N_{ij} is an array used to record the link (population) index (i.e., the serial number of the wavelength/waveband occupied by the link) on ES_{ij}. We run the GREEDY algorithm sequentially over our constructed LAG and calculate a candidate path for each traffic request $r_{sd} \in R$. Finally, the generated initial set of candidate paths is the initial solution matrix (i.e., the ecological system):

$$HSI_{ij} = P\left(r_{ij}\right) / Q\left(r_{ij}\right) \tag{30}$$

where $P\left(r_{ij}\right)$ is the actual power consumption by the selected path ES_{ij} of the traffic request $r_{ij} \in R$; $Q\left(r_{ij}\right)$ is the SQSD of r_{ij}. We

a

b
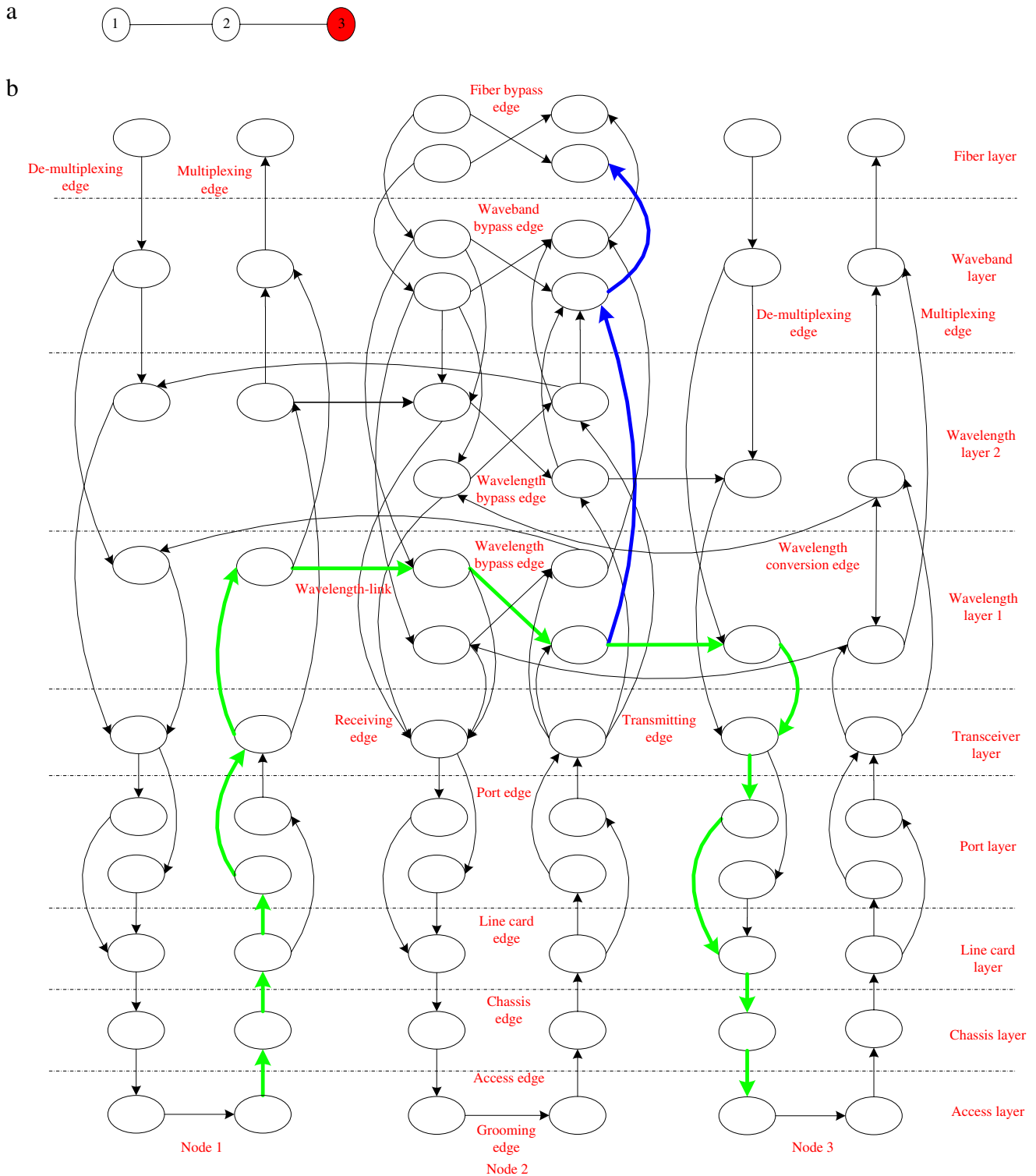
Fig. 3. Illustration of the LAG.

first construct the SQSDM $S_{QoS}^t(r_{sd})$ according to Eq. (16), and then calculate its average value $E\left[S_{QoS}^t(r_{sd})\right]$ and the deviation value $D\left[S_{QoS}^t(r_{sd})\right]$. Finally, we have

$$Q\left(r_{ij}\right) = E\left[S_{QoS}^t(r_{sd})\right]^{D\left[S_{QoS}^t(r_{sd})\right]}. \tag{31}$$

4.3. Migration

Migration is an important approach of exchanging the superior feature (i.e., the common links) among paths (habitats) and helps us to evolve the ecological system (solution matrix). We first rank the habitat suitability index (HSI) of ES_{ij} and determine if ES_{ij} needs to be processed by the migration. The following method is utilized

1    $Q(R) = E\left[S_{QoS}(R) \right]^{D\left[S_{QoS}(R) \right]}$;

2 **for** each $i \in V$ **do**

3   **for** each $j \in V$ **do**

4   **if** the path ES_{ij} is selected by a traffic request **then**

5   Update its link index in array N_{ij};

6   Insert the indices of the wavelengths/wavebands occupied by these links;

7   **if** multiple wavelength-routes share the common links **then**

8   Multiplex them into the corresponding waveband;

9   **end**

10   **end**

11   **end**

12 **end**

13 Update the device status;

14 $es' \leftarrow es$;

15   $C_p(R) = P(R)/P_{\max}$;

16   $GHSI(es') = \begin{cases} C_p(R)/Q(R), & es' \text{ is an available solution} \\ 0 & , \text{ others} \end{cases}$

Fig. 4. Pseudo code of updating *es*.

to obtain the evaluation rank of HSI for ES_{ij}. Given the size N of $ES_{|V|\times|V|}$, i.e., the total number of paths in the ecological system, N is just the highest rank K_{max}, which is owned by the path ES_{i*j*} with the largest HSI_{i*j*} in $ES_{|V|\times|V|}$. Then, we sort all the paths in $ES_{|V|\times|V|}$ according to HSI in descending order. Finally, starting from ES_{i*j*}, we set the corresponding evaluation rank k_{ij} for each path ES_{ij} in the order of decreasing K_{max} per time. Based on the given evaluation rank k_{ij}, we can calculate the immigration rate λ_{ij}^{in} and the emigration rate λ_{ij}^{out} for each path ES_{ij}. λ_{ij}^{in} measures the probability that some links on other paths (populations) are transferred into ES_{ij}. λ_{ij}^{out} measures the probability that ES_{ij} moves some links out into other paths. λ_{ij}^{in} and λ_{ij}^{out} are calculated as follows:

$$\lambda_{ij}^{in} = E \cdot \left(1 - \frac{k_{ij}}{K_{max}} \right) \tag{32}$$

$$\lambda_{ij}^{out} = \frac{L \cdot k_{ij}}{K_{max}} \tag{33}$$

where E and L are the maximum immigration rate and the maximum emigration rate, respectively.

Given the migration probability R_m, if $\lambda_{ij}^{in} > R_m$, we will perform the immigration operation on ES_{ij}. We use the following "roulette wheel" method to select the corresponding emigrating links for ES_{ij}. First, we sum up the emigration rates of other paths and calculate the range for each path on the wheel. Then, we generate a random decimal and see which range it falls into. The path associated with this range is selected as the emigration habitat. For example, the emigration rates of three paths are 0.4, 0.3, and 0.3, respectively. We first obtain three ranges [0, 0.4], [0.4, 0.7], and [0.7, 1] followed by the "roulette wheel" method above. If the random decimal is set by 0.75, the third path is selected as the emigration habitat. In this emigration path, we select the links with the same end nodes as emigrating links, and then they are immigrated into ES_{ij}. Thus, the migration of ES_{ij} is completed.

4.4. Mutation

After executing the migration among paths, if HSI_{ij} of the path ES_{ij} is still low, we infer that the path has low quality. In this

case, the operation of mutation should be implemented over ES_{ij} to enhance its link diversity. The mutation is expected to increase the probability that ES_{ij} is changed into a better path in the matrix. The mutation probability function $\gamma(ES_{ij})$ is used to determine whether the mutation operation needs to be performed over ES_{ij}. It is calculated as follows:

$$\gamma(ES_{ij}) = \gamma_{max} \cdot \left(1 - \frac{K_{ij}}{K_{max}} \right) \tag{34}$$

where γ_{max} is the maximum mutation probability. Given a random positive decimal σ, if $\gamma(ES_{ij}) > \sigma$, we will use Dijkstra's algorithm to recalculate a candidate path ES_{ij}' on our LAG for the traffic request r_{ij}. Thus, the mutation operation is completed for ES_{ij}.

4.5. Solution matrix update

Each time we get a new solution matrix (ecological system) es', we need to update the whole HSI of the ecological system to $GHSI(es')$. $GHSI(es')$ is used to evaluate the solution matrix es'. It is related to the total power consumption of network devices occupied by the selected paths of various traffic requests and the value of MQSD. It is calculated as below:

$$GHSI(es') = \begin{cases} C_p(R)/Q(R), & es' \text{ is an available solution} \\ 0, & \text{others} \end{cases} \tag{35}$$

Fig. 4 shows the pseudo code of updating *es* into *es'*.

4.6. GRG_BBO

Fig. 5 shows the pseudo code of GRG_BBO. The input parameters are *R*, *LAG*, *NE*, and R_m. *R* is the traffic matrix. *LAG* is the constructed layered auxiliary graph. *NE* denotes the maximum times of continuous iteration. R_m denotes the migration probability.

Lines 1–4 are for generating the initial solution *es* by the method in Section 4.2. Lines 9–14 are for performing the migration operations for the paths in the solution matrix *es* by the method in Section 4.3. Lines 15–21 are for performing the mutation operations for the paths in the solution matrix *es* by the method

```
Input: R, LAG, NE, R_m
Output: es'

1   for each traffic request  r_sd ∈ R   do

2       Find a candidate path over the LAG by GREEDY algorithm;
3   end
4   Combine these paths to form the initial solution es;

5    Calculate GHSI(es);

6   c = 0;
7   while c ≤ NE  do
8       Rank all the paths in es by their HSI values;
9       for each ES_ij ∈ es  do

10          Calculate the immigration rate  λ_ij^in   and the emigration rate  λ_ij^out ;

11          if  λ_ij^in > R_m   then

12              Perform migration operation for  ES_ij;
13          end
14      end
15      for each ES_ij ∈ es  do
16          Calculate its mutation probability  γ(ES_ij);
17          Generate a random positive decimal  σ;
18          if   γ(ES_ij) > σ  then
19              Perform mutation operation for  ES_ij;
20          end
21      end
22      es' ← es;

23      c=c+1;

24  end
25  return es';
```

Fig. 5. Pseudo code of GRG_BBO.

in Section 4.4. Line 22 is for generating the new ecological system es' and calculating the corresponding $GHSI(es')$ by the method in Section 4.5.

5. Performance evaluation

We have evaluated the performance of GRG_BBO through simulation experiments. For comparison purposes, we have identified two state-of-the-art heuristic algorithms for traffic grooming, i.e., THG (traditional hybrid grooming) [4] and PAHG (power aware hybrid grooming) [24]. Since our algorithm is based on the intelligent algorithm BBO, to guarantee the comparison fairness, we have also integrated the BBO part into THG and PAHG. Thus, two new counterpart algorithms, i.e., THG_BBO and PAHG_BBO, are developed in the simulation experiments against GRG_BBO.

All these three algorithms have similar complexity and overhead. The overhead of these algorithms mainly comes from two components. One is the route search on LAG and the other is BBO. Both THG and PAHG are actually kinds of greedy algorithms which select the available shortest path for each traffic request sequentially. The addition of BBO is to enhance the routing search capability. However, in GRG_BBO, the routing and traffic grooming are integrated. The BBO part helps to enhance the sharing of the common links for reducing the number of active components. Therefore, under the same complexity and overhead, we will investigate the performance of GRG_BBO against the other two algorithms in terms of the power consumption, QoS, and running time.

The implementation of GRG_BBO is an easy task. In BBO, each candidate path is regarded as a habitat and all the links on this path form the population. Therefore, no extra data structures are required. In GRG_BBO, the number of habitats is the same as the number of candidate paths. However, the number of candidate path is linearly related to the number of traffic requests. Therefore, the number of habitats is linearly related to the size of the traffic matrix. GRG_BBO has good scalability.

We use four topologies as shown in Fig. 6. These four topologies are SuperSINET of Japan, NSFNET of America, CERNET2 of China, and GéANT2 of Europe. The test topologies are assumed to have sufficient network resources. We compare the network power consumption and analyze the power consumption ratio of the device. $\forall v_i \in V, N_{chas}^{v_i} = 4, N_{lc}^{v_i.j} = 4, N_{port}^{v_i.j,k} = 4$. The other parameters are set in Table 3.

5.1. Comparison of network power consumption

Fig. 7 shows the comparison results of network power consumption for these three algorithms in different topologies. In each topology, the number of traffic requests is increased from 950 to 4000. The simulation results show that the network power consumption by using GRG_BBO is much lower than those of the

(a) SuperSINET.

(b) NSFNET.
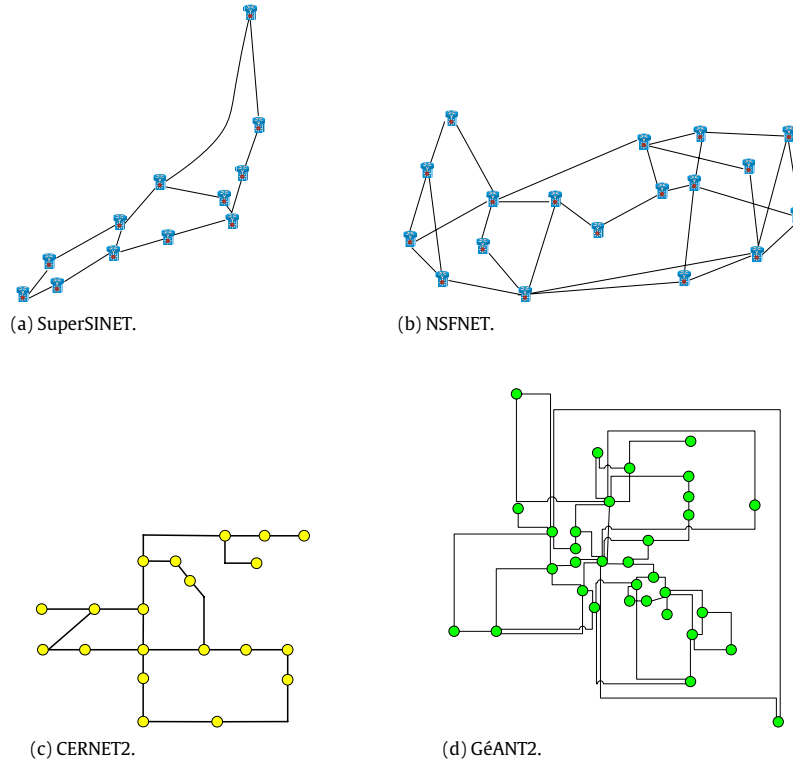
(c) CERNET2.

(d) GéANT2.

Fig. 6. Test topologies.
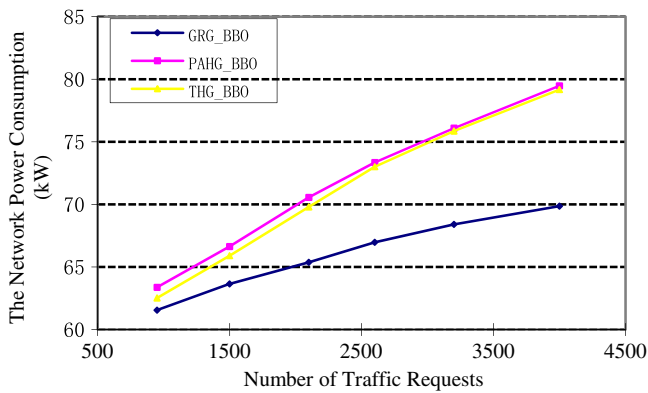
(a) Power consumption in SuperSINET.
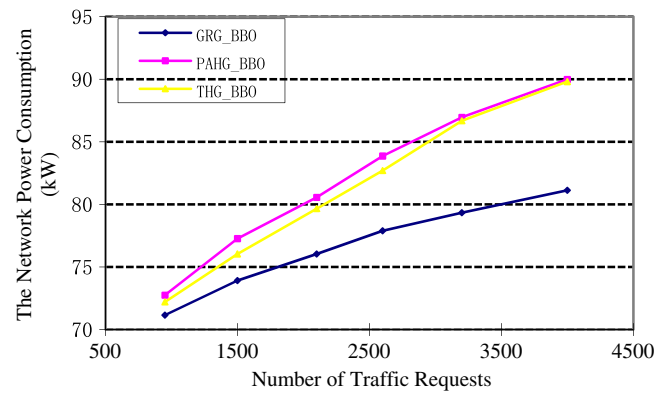
(b) Power consumption in NSFNET.
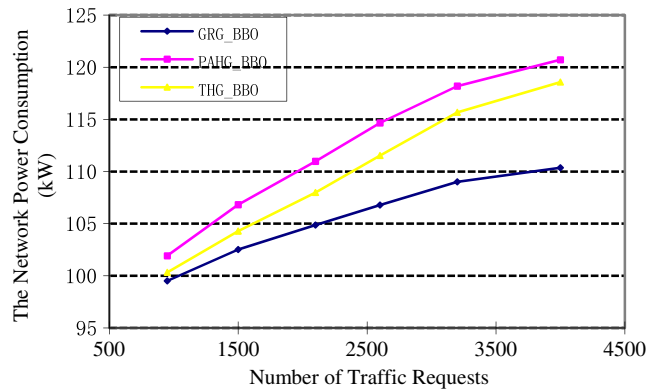
(c) Power consumption in CERNET2.
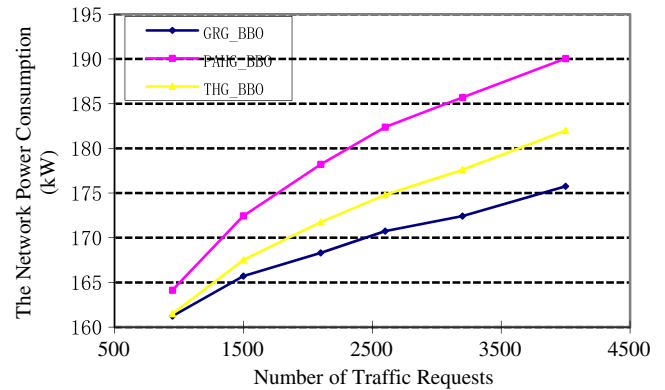
(d) Power consumption in GéANT2.

Fig. 7. Comparison of power consumption in the four topologies.

(a) Core router module.

(b) Transceiver.

(c) MG-OXC/OXC.

(d) Link component.
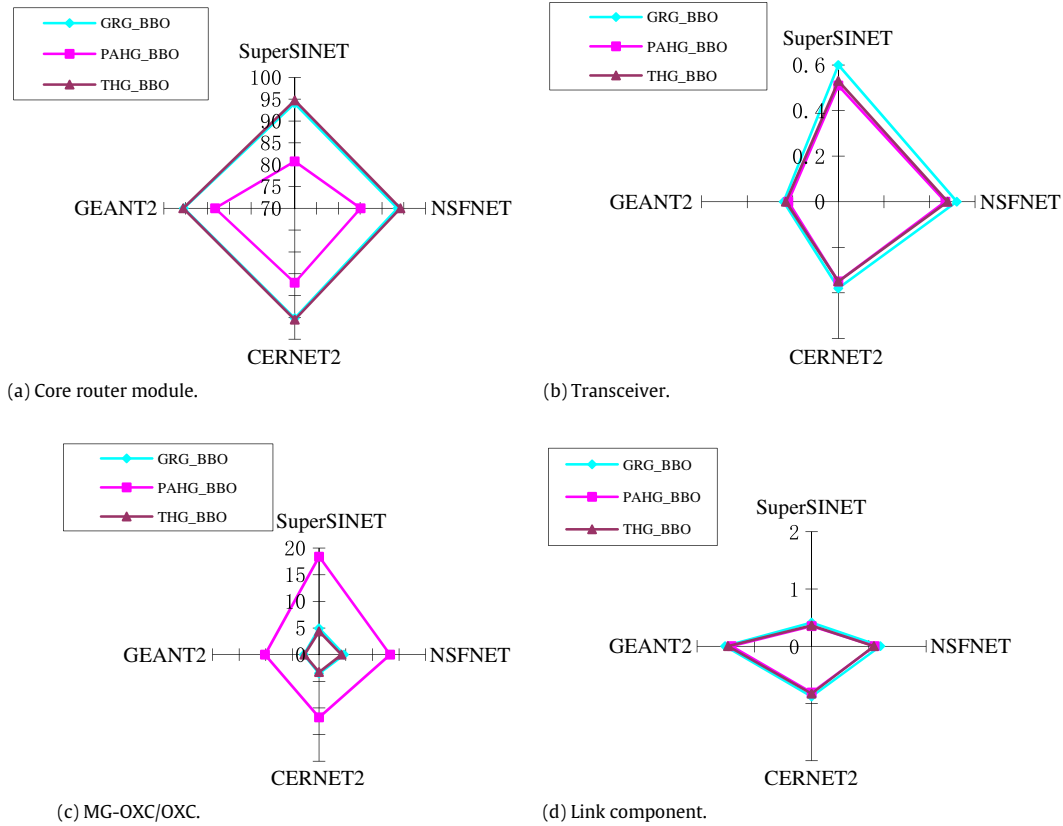
Fig. 8. The power consumption ratios of the different devices over various network topologies.

Table 3
Test parameters.

Name	Value	Name	Value
W	60	P_{port}^{wxc}	20W
WB	OC-768	P_{port}^{bxc}	20W
P_{ctr}^{cr}	356W	P_{port}^{fxc}	20W
P_{port}^{cr}	150W	P_{wc}	18W
P_t	3.5W	P_{pre}	4.8W
P_r	3.5W	P_{relay}	4.8W
P_{mux}	1W	P_{post}	4.8W
P_{demux}	1W	P_{rg}	26W

other two algorithms. Moreover, with the increasing number of traffic requests, the power saving becomes more and more evident. The improvement ratio is in the range of 2%–15%. The average improvement ratio is approximately 5%. It is expected since in PAHG_BBO, each wavelength-route consumes a large number of optical switching ports and the number of switching ports in use is significantly increased when more traffic requests arrive. By using THG_BBO, due to the fact that the chassis or line cards do not have the function of modularized management, the time and devices involved in active mode are increased significantly when more traffic requests arrive.

On the one hand, GRG_BBO utilizes the waveband switching technique and conducts the path migration operations based on the superior feature of common links. Thus, by using GRG_BBO, the multiple lightpaths with traversing the common links are merged into the waveband tunnel and transmitted as a single entity so that a quantity of optical switching ports are saved. Therefore, GRG_BBO has lower network power consumption than that of PAHG_BBO. On the other hand, in the novel node structure of MTN, the chassis, line cards, and ports all have the capability of power awareness and management, which increase the number of

components at idle states. Therefore, GRG_BBO has lower power consumption than that of THG_BBO as well.

As shown from Fig. 7, these three algorithms have produced significantly different power consumption over the four different topologies. The reason is due to that they have different network size. SuperSINET has 12 nodes. NSFNET has 18 nodes. CERNET2 has 20 nodes. GéANT2 has 33 nodes. More nodes lead to higher complexity of the network topology. Since the traffic requests are randomly generated, the lightpaths in larger networks are generally more complicated than the lightpaths in smaller networks. Therefore, the lightpaths in GéANT2 consume the most power whilst the lightpaths in SuperSINET consume the least power.

5.2. Analysis of the power consumption ratio of the devices

Fig. 8 shows the power consumption ratio of devices for each algorithm over different topologies when the number of traffic requests is set as 4×10^3. With the increase of the network size, the probability of the waveband merging is increased and the power consumption from the optical devices is thereby decreased. Thus, in Fig. 8(a), the power consumption ratio of the core router module rises up with the increase of the network size. Fig. 8(b) shows that the power consumption ratio of the optical transceivers in GRG_BBO is the highest. The reason is that the total network power consumption in GRG_BBO is the lowest although the power consumption of optical transceivers is equal in different algorithms under the same number of traffic requests. Thus, the power consumption ratio of optical transceivers in GRG_BBO is higher than the ratios in other algorithms over various topologies. Fig. 8(c) shows that the power consumption ratio of OXC in PAHG_BBO is significantly higher than the ratios in other algorithms. Since it has not exploited the waveband switching scheme, all the wavelength
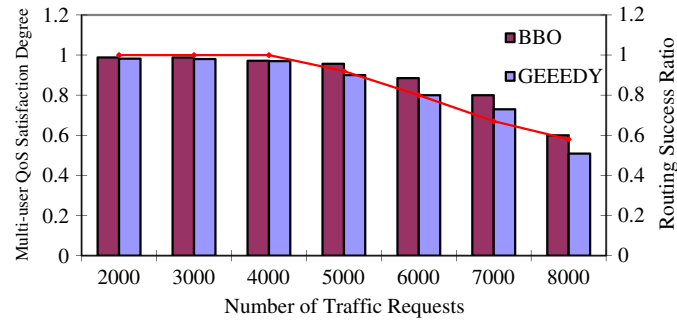
Fig. 9. Comparison of multi-user QoS satisfaction degree (denoted by columns) and routing success ratio (denoted by red curve).
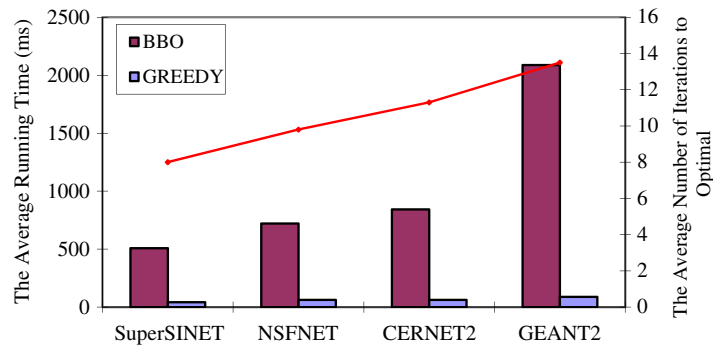
Fig. 10. Comparison of the average running time (denoted by columns) and the average number of iterations (denoted by red curve).

routes use a large number of OXC ports to transmit the traffic. Thus, the power consumption ratio of OXC is remarkably increased. Fig. 8(d) shows that the power consumption ratio of link devices in these algorithms rises up with the increase of the network size. This is because that the average path length is longer and thereby more link devices are traversed when the network size becomes larger.

5.3. BBO vs GREEDY

To evaluate the effectiveness of the BBO strategy, in addition to running the proposed algorithm based on BBO, we also run it based on the GREEDY strategy. Over CERNET2, we compare the performance of the algorithms between BBO and GREEDY with the increasing number of traffic requests. The performance metrics are multi-user QoS satisfaction degree (MQSD) and the routing success ratio. Fig. 9 plots the comparison results which show that when the number of traffic requests reaches a critical value, both MQSD and the routing success ratio decrease. The reduction of QoS satisfaction degree comes from the fact that the algorithm cannot find satisfactory paths for all the arrived traffic due to insufficient network resources.

We also note that BBO always performs better in terms of MQSD and routing success ratio. The contributions are made by the mutation operations in BBO, which can improve the path diversity and thereby provide a broader scope of paths selected for the user. Fig. 10 shows the comparison results of the average running time and the average number of iterations over four different topologies. We can see that the running time of BBO is much longer than that of GREEDY. With the increase of the network size, the number of iterations for reaching the optimal routing also increases. Therefore, a larger network size leads to longer running time of the algorithms. As future work, we will study how to reduce both the running time and the number of iterations.

6. Conclusions and future work

This paper aims to help build a cross-layer optimization based and power-efficient multi-granularity transport network. It first characterizes the traffic matrix to form the mapping between the user application type and QoS requirements. Two important metrics are introduced, i.e., the power consuming coefficient and multi-user QoS satisfaction degree, to comprehensively evaluate the performance of a power-efficient multi-granularity transport network. Based on the novel node structure, we construct the layered auxiliary graph to implement joint routing at both the IP layer and optical transport layer. The paths are calculated on the LAG. Furthermore, by using biogeography based intelligent optimization method BBO, we propose a green integrated routing and grooming algorithm called GRG_BBO.

By using GRG_BBO, the IP layer core router module has the capabilities of power awareness and management. GRG_BBO adjusts the status of chassis, line cards, and ports in response to the traffic load change. Thus, more chassis and line cards are turned into idle states to reduce the power consumption of IP layer devices. At the optical transport layer, the waveband switching is used to reduce the optical switching ports in use and the associated power consumption. By using the BBO strategy, the common links are regarded as a superior feature that is used in migration and mutation between various paths. The BBO strategy improves the hybrid grooming and waveband merging capabilities, provides the global optimization of the network power consumption and the user QoS satisfaction degree, and jointly optimizes the power efficiency at both the IP layer and optical transport layer. The simulation results demonstrate that compared to the existing state-of-the-art power-efficient routing algorithms, GRG_BBO achieves more power saving and provides higher quality of services to the users. The proposed GRG_BBO is an effective approach of helping design a power-efficient multi-granularity transport network.

There are two directions to carry on future work. One is to use other population-based artificial intelligence techniques to solve this problem. The popular population-based AI techniques include Genetic Algorithm, Ant Colony Optimization, Particle Swarm Optimization, etc. We can apply them to solve our routing and grooming problem separately. Extensive experiments will be conducted to compare them with GRG_BBO to see if further performance improvement can be achieved. The other direction is to change our optimization model from single-objective to multi-objective. For our problem, we have two optimization objectives, i.e., the power consuming coefficient and the multi-user QoS satisfaction degree. In this work, actually, we have combined them into a single metric. However, there are quite a few multi-objective optimization algorithms which have been proved successful in solving the other multi-objective optimization problems. We will then separate the two optimization problems in our problem and apply the multi-objective optimization algorithms to solve it. The results will be compared with the ones obtained by GRG_BBO for further analysis.

Acknowledgments

References

[1] Muhammad Ajmal, Monti Paolo, Cerutti Isabella, Wosinska Lena, et al., Energy-efficient WDM network planning with dedicated protection resources in sleep mode, in: Proc. GLOBECOM, 2010, p. 5.

[2] J. Baligan, K. Hinton, R. Tucker, Energy consumption of the internet, in: Proc. COIN/ACOFT, 2007, pp. 1–3.

[3] S. Blake, An Architecture for Differentiated Services, Internet RFC, RFC2475, 1998.

[4] X. Cao, V. Anand, C. Qiao, Waveband switching for dynamic traffic demands in multi-granular optical networks, IEEE/ACM Trans. Netw. 15 (4) (2007) 957–968.

[5] H.Y. Dong, M. Huang, The batch machine scheduling of continuous caster with flexible jobs to minimize setup costs, Concurrent Eng.-Res. A. 19 (4) (2011) 325–334.

[6] End-user multimedia QoS categories ITU-T G.1010, 2001.

[7] S. Guha, C. Chau, P. Basu, Green wave latency and capacity-efficient sleep scheduling for wireless networks, in: Proc. INFOCOM, 2010, p. 9.

[8] H. Gu, K. Mo, J. Xu, et al., A Low-power low-cost optical router for optical networks-on-chip in multiprocessor systems-on-chip, in: Proc. ISVLSI, 2009, pp. 19–24.

[9] L. Guo, X. Wang, W. Ji, et al., A new waveband switching method for reducing the number of ports in wavelength-division-multiplexing optical networks, Opt. Fiber Technol. 15 (1) (2009) 5–9.

[10] A. Hamad, A. Kamal, Routing and wavelength assignment with power aware multicasting in WDM networks, in: Proc. BROADNETS, 2005, pp. 31–40.

[11] M. Hasan, F. Farahmand, A. Patel, et al., Traffic grooming in green optical networks, in: Proc. ICC, May 2010, pp. 1–5.

[12] W. Hou, L. Guo, X. Wang, et al., A new multi-granularity traffic grooming routing algorithm in IP over WDM networks, Optik 122 (11) (2011) 1019–1029.

[13] M. Huang, F. Lu, W.-K. Ching, T.-K. Siu, A distributed decision making model for risk management of virtual enterprise, Expert Syst. Appl. 38 (10) (2011) 13208–13215.

[14] F. Idzikowski, S. Orlowski, et al., Dynamic routing at different layers in IP-over-WDM networks-Maximizing energy savings, Opt. Switching Networking 8 (2011) 181–200.

[15] F. Idzikowski, S. Orlowski, C. Raack, H. Woesner, A. Wolisz, Saving energy in IP-over-WDM networks by switching off line cards in low-demand scenarios, in: Proc. ONDM, 2010, p. 6.

[16] M. Lee, J. Yu, Y. Kim, et al., Design of hierarchical cross connect WDM networks employing a two-stage multiplexing scheme of waveband and wavelength, IEEE J. Sel. Area Comm. 20 (1) (2002) 166–171.

[17] Y.-L. Li, M. Huang, K.-S. Chin, X.-G. Luo, Y. Han, Integrating preference analysis and balanced scorecard to product planning house of quality, Comput. Ind. Eng. 60 (2) (2011) 256–268.

[18] M. Li, B. Ramamurthy, Dynamic waveband switching in WDM mesh networks based on a generic auxiliary graph model, Photonic Netw. Commun. 10 (3) (2005) 309–331.

[19] J. Lu, H. Wang, D. Tong, et al., A NoC router design supporting quality-of-service, J. Comput. Aid. Design Comput. Graphics 20 (11) (2008) 1403–1410.

[20] R. Parthiban, R. Tucker, C. Leckie, Waveband grooming and IP aggregation in optical networks, J. Lightwave Technol. 21 (11) (2003) 2476–2488.

[21] L. Saker, S.E. Elayoubi, T. Chahed, Minimizing energy consumption via sleep mode in green base station, in: Proc. WCNC, 2010, p. 6.

[22] G. Shen, R. Tucker, Energy-minimized design for IP over WDM networks, IEEE/OSA Journal of Optical Communications and Networking 1 (1) (2009) 176–186.

[23] D. Simon, Biogeography-based optimization, IEEE Trans. Evolut. Comput. 12 (6) (2008) 702–713.

[24] R S. Tucker, Optical packet-switched WDM networks: a cost and energy perspective, in: Proc. 2008 Conference on Optical Fiber Communication/National Fiber Optic Engineers Conference, San Diego, CA, USA, 2008.

[25] W. Vereecken, L. Deboosere, et al., Energy efficiency in telecommunication networks, in: Proc. NOC, 2008, pp. 176–186.

[26] A. Vince, A framework for the greedy algorithm, J. Discrete Appl. Math. 121 (1–3) (2002) 247–260.

[27] X. Wang, W. Hou, L. Guo, et al., Energy saving and cost reduction in multi-granularity green optical networks, Comput. Netw. 55 (3) (2011) 807–821.

[28] X. Wang, W. Hou, L. Guo, et al., A new multi-granularity grooming algorithm based on traffic partition in IP over WDM networks, Comput. Netw. 55 (3) (2011) 676–688.

[29] Y. Wu, L. Chiaraviglio, Mellia M, et al., Power-aware routing and wavelength assignment in optical networks, in: Proc. ECOC, 2009, pp. 1–2.

[30] M. Xia, M. Tornatore, Y. Zhang, et al., Green provisioning for optical WDM networks, IEEE J. Sel. Top. Quant. 17 (2) (2011) 437–445.

[31] E. Yetginer, G. Rouskas, Power efficient traffic grooming in optical WDM networks, in: Proc. GLOBECOM, Jun. 2009, pp. 1838–1843.

[32] Donggyu Yun, Jihyeong Lee, Yung Yi, Research in green network for future internet, J. KIISE 28 (1) (2010) 41–51.

Xingwei Wang received the Ph.D. degree in computer science from Northeastern University, Shenyang, China, in 1998. He is currently a professor in the Faculty of Information Science and Engineering, Northeastern University. His research interests include resource management for cloud computing, optimized routing algorithms in new generation Internet and future Internet.

Hui Cheng received the B.Sc. and M.Sc. degrees in computer science from Northeastern University, China in 2001 and 2004, and the Ph.D. degree in computer science from The Hong Kong Polytechnic University, Hong Kong in 2007. He is currently a lecturer in the Department of Computer Science and Technology at the University of Bedfordshire, Luton, United Kingdom. His research interests include artificial intelligence, dynamic optimization, optical networks, mobile ad hoc networks, and QoS routing. He has published over 40 technical papers in the above areas.

Keqin Li is a SUNY Distinguished Professor of computer science in the State University of New York at New Paltz. He is also an Intellectual Ventures endowed visiting chair professor at the National Laboratory for Information Science and Technology, Tsinghua University, Beijing, China. His research interests are mainly in design and analysis of algorithms, parallel and distributed computing, and computer networking. His current research interests include lifetime maximization in sensor networks, file sharing in peer-to-peer systems, power management and performance optimization, and cloud computing. Dr. Li has published over 250 journal articles, book chapters, and research papers in refereed international conference proceedings. He has received several Best Paper Awards for his highest quality work.

Jie Li received the B.E. degree in computer science from Zhejiang University, Hangzhou, China, and the M.E. degree in electronic engineering and communication systems from the China Academy of Posts and Telecommunications, Beijing, China. He received the Dr. Eng. degree from the University of Electro-Communications, Tokyo, Japan. His research interests are in mobile distributed computing and networking, OS, network security, modeling and performance evaluation of information systems. He received the best paper award from IEEE NAECON'97. He is a senior member of IEEE and ACM, and a member of IPSJ (Information Processing Society of Japan).

Jiajia Sun received the Bachelor degree in computer science and technology from Northeastern University, Shenyang, China, in 2012. She is now studying for the Master degree of computer application technology in Northeastern University. Her research interests include resource management for cloud computing and social cloud.